Sliding Viscoelastic Contacts: The Role of Adhesion, Boundary Conditions, and Finite Geometry

Sliding viscoelastic contacts: The role of adhesion, boundary conditions, and finite geometry

Luciano Afferrante[1*], Guido Violano[1] and Giuseppe Demelio[1]

[1*]Department of Mechanics, Mathematics and Management, Polytechnic University of Bari, Via E. Orabona 4, Bari, 70125, Italy.

*Corresponding author(s). E-mail(s): luciano.afferrante@poliba.it; Contributing authors: guido.violano@poliba.it; giuseppepompeo.demelio@poliba.it;

Abstract

In this study, we investigate the tangential sliding of a rigid Hertzian indenter on a viscoelastic substrate, a problem of practical interest due to the crucial role that sliding contacts play in various applications involving soft materials.
A finite element model is developed, where the substrate is modeled using a standard linear viscoelastic model with one relaxation time, and adhesion is incorporated using a Lennard-Jones potential law. We propose an innovative approach to model tangential sliding without imposing any lateral displacement, thereby enhancing the numerical efficiency. Our goal is to investigate the roles of adhesive regimes, boundary conditions (displacement and force-controlled conditions), and finite thickness of the substrate.
Results indicate significant differences in the system's behaviour depending on the boundary conditions and adhesion regime. In the short-range adhesion regime, the contact length $\boldsymbol{\mathcal{L}}$ initially increases with sliding speed before decreasing, showing a maximum at intermediate speeds. This behaviour is consistent with experimental observations in rubber-like materials and is a result of the transition from small-scale to large-scale viscous dissipation regimes. For long-range adhesion, this behaviour disappears and $\boldsymbol{\mathcal{L}}$ decreases monotonically with sliding speed.
The viscoelastic friction coefficient $\boldsymbol{\mu}$ exhibits a bell-shaped curve with its maximum value influenced by the applied load, both in long-range and short-range adhesion. However, under displacement control, $\boldsymbol{\mu}$ can be unbounded near a specific sliding speed, correlating with the normal force crossing zero.
Finally, a transition towards a long-range adhesive behaviour is observed when reducing the thickness $\boldsymbol{t}$ of the viscoelastic layer, which is assumed to be bonded to a rigid foundation. Moreover, the friction coefficient reduces when $\boldsymbol{t}$ tends to zero.

These findings provide insights into the viscoelastic and adhesive interactions during sliding, highlighting the critical influence of boundary conditions on contact mechanics.

Keywords: Adhesion, Viscoelasticity, Sliding, Friction coefficient, Finite Thickness

1 Introduction

The study of sliding contacts plays a crucial role in various applications involving soft materials. Examples include the tire industry, where contact with road surfaces is essential for traction [1, 2]; medical applications and coatings, where biocompatibility and wear resistance are vital [3, 4]; biology and biomimetics, which often mimic natural sliding mechanisms [5, 6]; micro and nano electro-mechanical systems, where precise control of sliding and friction is needed [7, 8]; haptic devices, which rely on tactile feedback [9, 10]; and soft bearings and gears used in robotics and machinery [11].

Soft matter frequently exhibits viscoelastic properties, combining both elastic and viscous behaviours, with response to stress or strain changing over time [12]. Consequently, modeling the contact mechanics of soft matter necessitates complex dynamic models that cannot rely on the quasi-static assumptions that have underpinned contact mechanics for over a century [13–15].

Among the first significant contributions to the study of tangential viscoelastic contacts, Hunter [16] proposed a solution to the problem of a rigid cylinder rolling on the surface of a viscoelastic solid. Introducing viscoelastic effects disrupts the symmetry present in the corresponding elastic problem, resulting in a resistive force that hinders the cylinder's motion. For a standard linear solid, the coefficient of friction, which depends on the rolling speed V_{s}, approaches zero at both very low and very high velocities, reaching a maximum at an intermediate speed.

Margetson [17] formulated a boundary-value problem for the rolling contact of a rigid cylinder over a viscoelastic layer bounded on a rigid foundation. In the range of investigated parameters, the results indicated that for a fixed contact area, during steady rolling, reducing the thickness of the viscoelastic layer increases both the normal and tangential forces. However, this reduction in thickness also leads to a decrease in the friction coefficient.

More recently, Persson [18] developed a versatile approach, applicable to materials with any viscoelastic modulus, including those measured experimentally. This theory can be applied to both spheres and cylinders rolling on semi-infinite viscoelastic solids or on a thin viscoelastic film adhered to a rigid flat substrate.

Menga et al. [19] investigated the sliding contact between a rigid sinusoid and a viscoelastic half-space, expanding upon Hunter's approach for cylindrical contacts [16]. Their research unveiled a transition from full to partial contact depending on the applied load and sliding speed. This phenomenon, which is not observed in smooth single asperity contacts, is influenced by the viscoelastic stiffening of the material and the periodic nature of the contact. This study has also been extended to examine the sliding contact of viscoelastic layers on rigid rough profiles [20], a problem that is of great interest in the context of rubber friction [21, 22].

The aforementioned studies focus on sliding contact without considering adhesive interactions. However, in soft matter contacts, macroscopic adhesion is frequently observed [23–26]. The importance of adhesion is also evidenced by the numerous recent theoretical studies on adhesive contact between viscoelastic bodies [27–31]. Many of these studies have focused only on normal contact problems, where energy dissipation occurs in a loading-unloading cycle, originating from both interface adhesion and bulk material viscoelasticity [32].

Violano & Afferrante [33] demonstrated that the interplay between adhesion and viscoelasticity can significantly influence adhesive behavior, a phenomenon that is less evident in situations with long-ranged interactions. Long-range adhesion typically characterizes stiff materials, where adhesive interactions prevail outside the contact area [34–36]. Conversely, compliant materials typically exhibit short-range adhesion, with adhesive forces primarily acting within the contact region [37, 38]. The transition between long and short-range adhesion is governed by the Tabor parameter [39], which is well-defined in the context of elastic Hertzian contacts. However, establishing a definitive definition for the Tabor parameter remains challenging, particularly in scenarios involving viscoelasticity [33] and/or surface roughness [40, 41].

In a recent study, Perez-Rafols & Nicola [42] investigated the sliding tangential contact between a smooth cylinder and a flat surface in the framework of linear elasticity, by considering the presence of both adhesion and friction. In particular, they explored the effect of the Tabor parameter. Their findings revealed that under long-range adhesion conditions, the contact pressure retains a relatively steady profile, whereas in scenarios characterized by short-range adhesion, a pressure spike manifests at the contact edge.

Carbone et al. [30, 43] introduced a boundary formulation based on Green's function approach, to study the adhesive contact of linear viscoelastic materials in steady-state sliding against rough substrates. Their results indicate that viscoelasticity may affects the adhesive response depending on the sliding speed. Additionally, the interaction between adhesion and viscoelasticity plays a significant role in determining the overall frictional behavior.

Papangelo et al. [44] considered the effect of the Tabor parameter in the problem of a sliding viscoelastic cylinder in presence of adhesion. They showed that the friction coefficient depends on four dimensionless parameter. Moreover, they observed that for small Tabor parameter the solution tends to Hunter's adhesiveless prediction [16].

Current research on adhesion between viscoelastic materials often employs the 'half-space approximation', where one of the interacting bodies, typically the deformable viscoelastic one, is assumed to be infinitely tall. This assumption is questionable when the contact area becomes of the same order of magnitude of the size of contacting bodies [45]. Finite-size effects can significantly influence both adhesive and viscoelastic behaviors [46]. Despite the practical relevance of systems with finite dimensions, there are few studies in the literature that explore the interplay between adhesion, viscoelasticity, and finite-size effects. Furthermore, existing contributions tend to concentrate solely on the normal contact case [46–48].

The context described highlights that there's a lack of a comprehensive model within the field of tangential sliding contacts that effectively integrates the interactions among adhesion and viscoelasticity, and the influence of boundary conditions.

The current study builds upon the finite element model established in Ref. [28], which incorporates adhesive interactions via a Lennard-Jones surface potential and employs the Maxwell representation of viscoelasticity. Specifically, we delve into the adhesive tangential sliding of a rigid Hertzian indenter on a viscoelastic substrate, with a primary focus on assessing the influence of different boundary conditions. Our study assumes frictionless contact, as it is not straightforward to separate the contribution of material dissipation from that of Coulomb friction to the overall friction resistance. Therefore, similar to recent studies [19, 20, 49] we omit the shear-related losses due to the adhesive tangential effects that occur during tangential displacements. In this context, it is worth noting that cohesive zone models (CZMs) incorporating both adhesion and friction have been proposed in the literature to account for the coupling of normal and tangential interface failure (see, for example, Ref. [50] and reference therein).

Finally, we highlight that a key innovation of our work lies in the novel approach used to streamline the numerical solution of the sliding problem by simulating the tangential displacement of the indenter through vertical movements of its nodes. This enhances computational efficiency compared to an equivalent FEM approach that applies an actual tangential displacement to the indenter.

2 The Model

A line contact problem is investigated. Specifically, we consider a rigid Hertzian indenter a rigid Hertzian indenter of radius of curvature R in sliding contact at constant velocity with a substrate made of linear viscoelastic material and in presence of adhesion. The geometry of the system is illustrated Fig. 1, where the geometric parameters governing the problem are indicated.

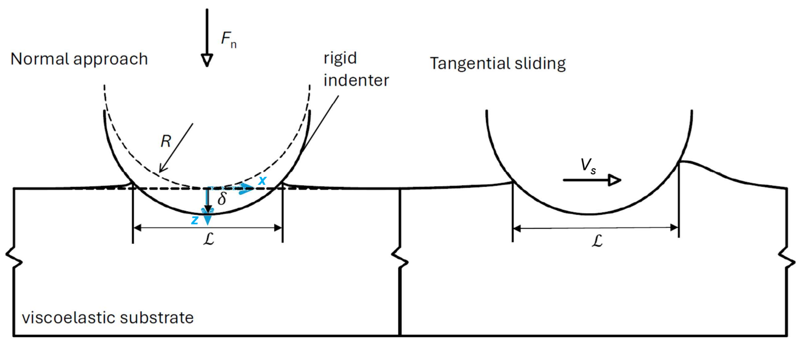

Fig. 1 The line contact problem investigated in the present work: A rigid Hertzian indenter of radius R is pressed into a viscoelastic substrate and then moved tangentially at fixed sliding speed V_s.

For the substrate material, we adopt a linear standard viscoelastic model with one relaxation time $\tau = 10^{-4}$ s and a ratio of low to high-frequency modulus $E_0/E_\infty = 0.1$. Specifically, the Maxwell representation is used with one spring (E_0) in parallel with a dashpot ($(E_0 - E_\infty)/\tau$) which is in turn in series with another spring ($E_0 - E_\infty$).

The contact problem is solved using the finite element (FE) strategy developed in Ref. [28], where the reader can find the details of the model. Here, we recall that the Derjaguin's approximation [51] is adopted to model the the surface interactions by using the traction-gap relation based on Lennard-Jones potential law

$$p_{\mathrm{LJ}} = \frac{8\Delta\gamma}{3\epsilon}\left[\left(\frac{\epsilon}{g}\right)^3 - \left(\frac{\epsilon}{g}\right)^9\right] \tag{1}$$

where g is the local gap between the surfaces, ϵ is the range of action of van der Waals forces, and $\Delta\gamma$ is the adiabatic surface energy of adhesion.

The simulation is divided in two phases. First, all the nodes of the indenter are uniformly approached to the substrate with a negligible vertical speed V_n, until a fixed maximum penetration δ (or load F) is reached. The condition $V_n \approx 0$ ensures that the process is quasi-static, with negligible viscous effects.

In the second phase, tangential sliding is simulated by conveniently moving in the vertical direction the nodes of the Hertzian punch, as schematically depicted in Fig. 2. This methodology significantly simplifies the numerical solution of the sliding problem as we do not need to apply any tangential displacement, making the code very efficient compared to a FEM approach where an actual tangential displacement is applied to the indenter.

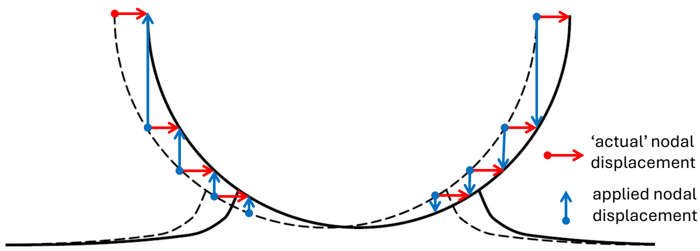

Fig. 2 A schematical representation of the methodology adopted to move horizontally the rigid indenter. The tangential displacement is reproduced by conveniently moving the nodes of the indenter in the vertical direction.

Moreover, depending on whether sliding occurs under fixed normal displacement or load, the substrate is either constrained at its base or subjected to the total load calculated at the end of the initial normal approach. Therefore, in the sliding simulations performed under controlled normal load conditions, the constant normal force maintained during the sliding phase is the one reached at the end of the approach phase, which is carried out under controlled normal displacement conditions. Consequently, the value of the normal force during sliding is not fixed a priori but is determined by regulating the final depth of penetration of the Hertzian indenter.

3 Results

All results showed in this section are obtained for a standard linear viscoelastic model with $E_0/E_\infty = 0.1$, nearly incompressible material (Poisson's ratio $\nu = 0.49$), and Tabor parameter, calculated with respect to the low frequency modulus E_0, $\mu_T = (R\Delta\gamma^2/E_0^{*2}\epsilon^3)^{1/3} = 1$ (long-range adhesion regime) and $\mu_T = 6.08$ (short-range adhesion regime). The quantity $E_0^* = E_0/(1-\nu^2)$ is the plain strain elastic modulus. In this regard, we must observe that the Tabor parameter should, in principle, be considered a function of the sliding speed, as we are dealing with viscoelastic materials whose modulus depends on the frequency of excitation. Specifically, at high sliding velocities, the definition of μ_T should be based on the high frequency modulus E_∞.

Furthermore, results are given in terms of the following dimensionless quantities: sliding speed $\hat{V}_s = V_s\tau/\epsilon$, contact length $\hat{\mathcal{L}} = \mathcal{L}/R$, penetration $\hat{\delta} = \delta/\epsilon$, contact force $\hat{F} = F/(\pi\Delta\gamma^2 E_0^* R)^{1/3}$, and pressure $\hat{p} = p/\sigma_{\max}$, being $\sigma_{\max} = 16\Delta\gamma/(9\sqrt{3}\epsilon)$ the Lennard-Jones tensile peak stress.

Determining the contact length $\mathcal{L}$ becomes complex when cohesive laws, like the Lennard-Jones force law used in this study, describe the interactions at the interface between contacting bodies. In a traditional Hertzian contact problem without adhesion, the contact area is clearly defined by the region where the pressure is compressive (positive) and the gap is zero. However, in the presence of adhesion, this definition loses its clarity, as the pressure can become tensile (negative) while the gap is still positive. Thus, a different approach to defining the contact area is required. Greenwood [52] suggested defining the contact area by the points where the tensile stress reaches its maximum. This approach has proven to be consistent and accurate in the short-range adhesion regime ($\mu_T >> 1$) as demonstrated by Feng [53]. Feng verified that, for $\mu_T > 1$, the boundaries of the flattened region between the contacting surfaces correspond well with the points of maximum tensile stress. For a small Tabor parameter $\mu_T < 0.1$, the edges of the flattened area are harder to identify and do not necessarily align with the points of peak tensile stress. Consequently, the definition of the contact area varies depending on the value of μ_T. In a subsequent work, Feng [54] showed that as long as the Tabor parameter $\mu_T > 0.1$, the deformed profiles indicate the presence of a flattened region at the contact interface, where the gap remains almost constant and the pressure peaks at the edges. Therefore, in this regime, we can define a gap threshold below which points are considered to be in contact. This threshold should be on the order of the length scale of the adhesive forces. In this study, we have set the gap threshold to 1.2ϵ as the reference value for determining contact points. Furthermore, it has been observed that in all simulations conducted in this study, the Tabor parameter consistently exceeds 0.1, regardless of the speed (and hence the excitation frequency depends), even in simulations assumed to be in the long-range adhesion regime.

It is important to specify that all results are presented under steady-state conditions, which are reached after an initial transient phase occurring at the beginning of the sliding.

Furthermore, in the present work, the friction coefficient is calculated as $\mu = |F_t/F_n|$ (see, for example, Refs. [21, 49, 55, 56]), being F_n the normal force and F_t the tangential force opposing the sliding motion and evaluated by

$$F_t = -\int_{\mathcal{L}} p(x) \frac{\partial u}{\partial x} dx, \tag{2}$$

where we denoted with u the normal displacement at the contact interface.

Regarding the friction coefficient μ, to demonstrate the accuracy of our methodology in simulating tangential displacement, we preliminary present in Fig. 3 a comparison between our FEM calculations and the BEM results reported in Ref. [44]. The agreement is nearly perfect. Furthermore, we observe that the initial increase in the friction coefficient at slow speeds follow the same trend observed in the rolling resistance data from experimental tests, which involved a PMMA cylinder rolling against an SBR plate under constant normal load [57].

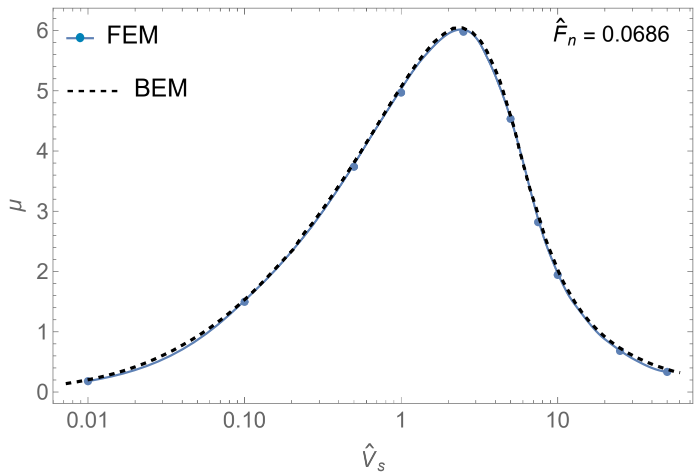

Fig. 3 The viscoelastic friction coefficient μ as a function of the adimensional sliding speed $\hat{V}_s$. A comparison is made between FEM and BEM calculations. The plots are obtained under force-controlled conditions, with a Tabor parameter $\mu_T = 6.08$ (corresponding to a Maugis paramenter $\lambda = 1.0264\mu_T = 3$). Data for the BEM curve are taken from Fig. 5g of Ref. [44] and are scaled to match the normalization adopted in the present paper.

3.1 Effect of the range of adhesion

First, we investigate the effect of adhesion range, focusing on both short-range and long-range adhesion. Short-range adhesion is particularly relevant for soft matter applications, where the material's compliance results in strong adhesion within the contact area. Conversely, long-range adhesion is typical for stiffer contacts, where adhesive interactions extend outside the contact region.

Unless otherwise specified, simulations are performed under fixed normal displacement. This means that the maximum penetration achieved at the end of the normal approach phase is kept constant during the tangential sliding.

Figures 4a-b show the normalized contact length $\hat{\mathcal{L}}$ given in terms of the imposed adimensional sliding speed $\hat{V}_s$. Results are given for different values of the approach $\hat{\delta}$. In long-range adhesion regime (Fig. 4a), the contact length decreases monotonically with velocity. Moreover, the elastic solution is recovered in the limit of low and high speed, with a smaller contact length at high velocity due to the increased viscoelastic modulus, which makes stiffer the substrate. Indeed, an increase in sliding speed results in a higher excitation frequency and, consequently, a higher viscoelastic modulus, which increases from the low-frequency value E_0 at negligible speeds to the high-frequency value E_∞ at very high speeds.

In the short-range regime, the behaviour of the contact length with velocity changes significantly.

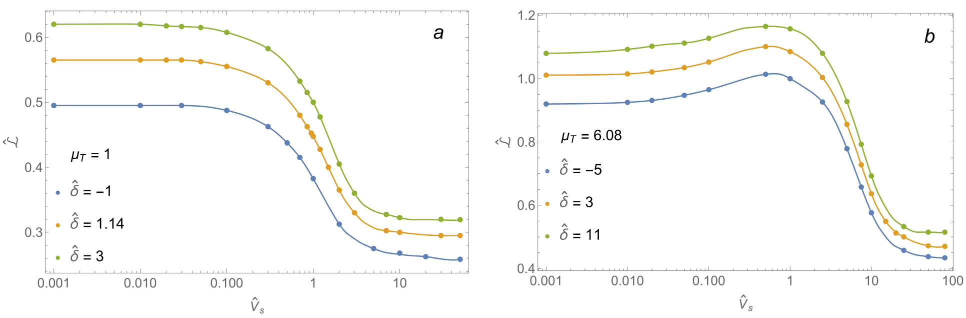

Fig. 4 The normalized contact length $\hat{\mathcal{L}}$ as a function of the adimensional sliding speed $\hat{V}_s$, for different values of the normal approach $\hat{\delta}$. Plots are obtained under displacement-controlled conditions, and Tabor parameter $\mu_T = 1$ (a) and $\mu_T = 6.08$ (b). Solid circles represent numerical data returned by FEM simulations, while solid lines are obtained through a spline interpolation of these data.

As shown in Fig. 4b, at intermediate sliding speeds, the contact area shows a maximum, despite the increasing viscoelastic modulus makes the substrate stiffer, and then decreases with V_s. This behaviour aligns with experimental tests of rolling contact conducted on rubber-like material [58, 59] and the theoretical findings of Carbone et al. [30, 43] who studied a similar issue for a sinusoidal-shaped indenter in the short-range adhesion regime. In their work, they also explain why the contact area initially increases before decreasing. In the context of short-range adhesion, two distinct sub-regimes emerge based on sliding speed: one characterized by minor viscous dissipation, occurring at speeds up to values on the order of $\hat{V}_s = 1$, and the other by significant viscous dissipation at higher speeds. At lower speeds, the primary viscous energy losses are concentrated at the rear edge of the contact zone, where the excitation frequency is considerably higher than in the substrate's bulk, which responds elastically with a modulus E_0. Conversely, at higher speeds, the viscoelastic energy losses within

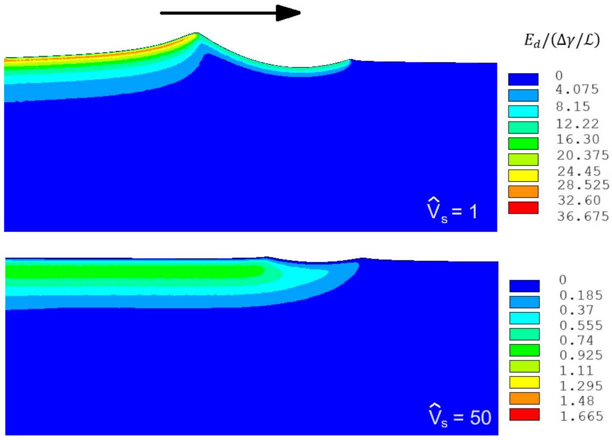

Fig. 5 The distribution of the viscoelastic dissipated energy per unit area E_d, normalized by $\Delta\gamma/\mathcal{L}$, in the short-range regime ($\mu_T = 6.08$) for two different speeds, $\hat{V}_s = 1$ and $\hat{V}_s = 50$. Results are presented once steady-state conditions are reached. Arrow indicates the sliding direction.

the bulk material become more pronounced. Under these conditions, the bulk material predominantly dissipates energy, while the contact region's edges exhibit elastic behaviour with a modulus E_∞.

This scenario is illustrated in Fig, 5, where the viscoelastic dissipated energy per unit area, normalized by $\Delta\gamma/\mathcal{L}$, is shown in the short-range regime for two different velocities. It is calculated as the energy required to deform the dashpot in the Maxwell element. At $\hat{V}_s = 1$, dissipation is clearly localized on the surface at the trailing edge, while at $\hat{V}_s = 50$, dissipation occurs subsurface, i.e., it moves into the bulk, and is several order of magnitude lower, practically negligible. Note that the legend scale of the two plots was chosen differently to allow visualization of the dissipation zones in both cases. Finally, we observe that the small-scale viscoelasticity regime is not observed in the long-range adhesion scenario, where the effects of adhesive forces are mainly localized outside the contact region. Therefore, in the long-range regime, viscous dissipation primarily occurs in the bulk material (see also Ref. [33]) and reaches significantly lower values regardless of the sliding speed.

In the present problem, the rigid Hertzian indenter is assumed to slide frictionlessly on the substrate. However, due to the deformation occurring during the sliding contact, dissipation within the viscoelastic material leads to an asymmetrization of the contact pressure, as displayed in Figs. 6a-b, where we plot the steady state adimensional contact pressure distribution $\hat{p}$ for different values of the sliding speed. In this case, results are provided for a fixed value of the normal force F_n, under both long-range (a) and short-range (b) adhesive regimes. In the extreme cases of zero and very high sliding speeds, the pressure distribution is symmetric, reflecting the elastic solutions. However, at intermediate speeds, where viscous dissipation occurs, the pressure distribution becomes asymmetric. Transitioning from short-range to long-range adhesion regimes, the tensile (negative) pressure peak is smoothed.

The asymmetric pressure distribution, in turn, results in the emergence of a tangential force F_t, commonly referred to as the viscoelastic friction force, that opposes the sliding motion, and typically calculated according to eq. (2).

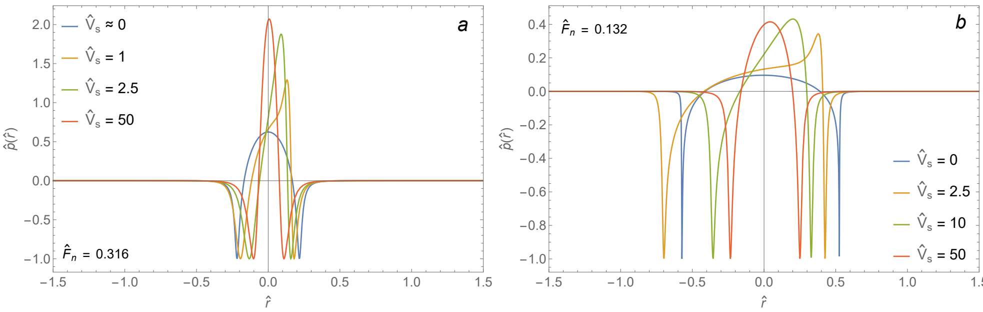

Fig. 6 The steady state adimensional pressure distribution $\hat{p}$, on the contact region, for different values of the sliding speed. Results are obtained under force-controlled conditions, and and Tabor parameter $\mu_T = 1$ (a) and $\mu_T = 6.08$ (b).

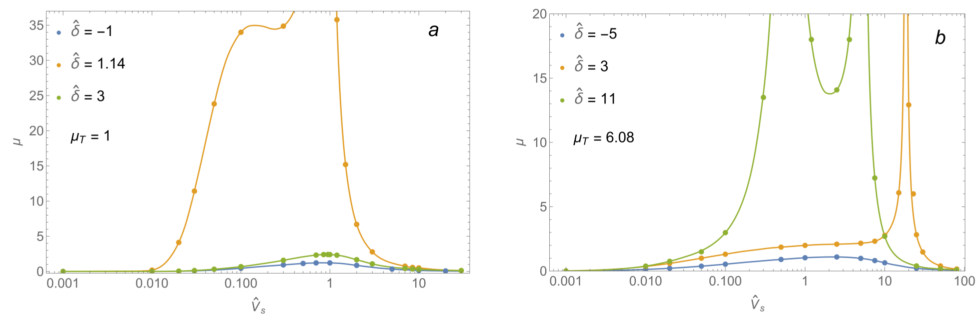

Fig. 7 The viscoelastic friction coefficient μ as a function of the adimensional sliding speed $\hat{V}_s$, for different values of the normal approach $\hat{\delta}$. Plots are obtained under displacement-controlled conditions, and Tabor parameter $\mu_T = 1$ (a) and $\mu_T = 6.08$ (b).Solid circles represent numerical data returned by FEM simulations, while solid lines are obtained through a spline interpolation of these data.

Figures 7a-b show the viscoelastic friction coefficient $\mu = |F_t/F_n|$ given in terms of the adimensional sliding speed $\hat{V}_s$ for long-range (a) and short-range (b) adhesive regimes and at different values of the imposed normal approach. Notably, the friction coefficient becomes unbounded at specific speeds. This occurs because, at these velocities, the normal force changes from negative to positive values, effectively passing through zero. This phenomenon is illustrated in Fig. 8, where both the friction force $\hat{F}_t$ and normal force $\hat{F}_n$ are presented as functions of the sliding speed for short-range adhesive conditions. Specifically, the green curve of Fig. 8b, corresponding to the adimensional approach $\hat{\delta} = 11$, passes twice through the zero, so explaining why the friction coefficient depicted by the green curve of Fig. 7b has two vertical asymptotes. Finally, note in Fig. 8a the friction force exhibits a bell-shaped trend regardless of the value of the approach and, as expected, continuously increases with δ.

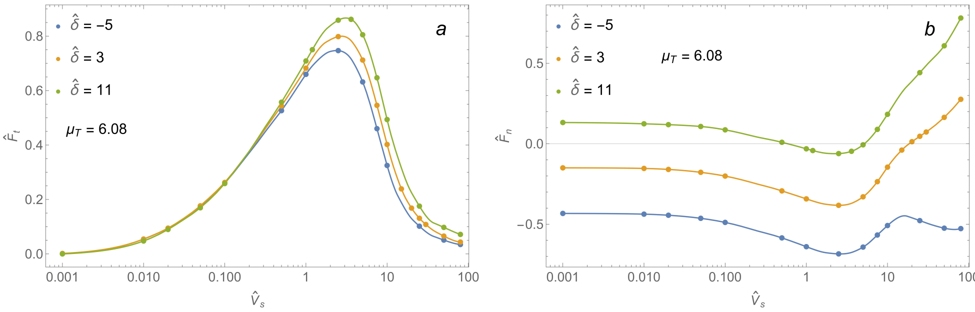

Fig. 8 The adimensional tangential force $\hat{F}_t$ (a), and normal force $\hat{F}_n$ (b) as a function of the adimensional sliding speed $\hat{V}_s$ for different values of the normal approach $\hat{\delta}$. Plots are obtained under displacement-controlled conditions, and Tabor parameter $\mu_T = 6.08$. Solid circles represent numerical data returned by FEM simulations, while solid lines are obtained through a spline interpolation of these data.

3.2 Effect of the normal boundary conditions

In the previous section, we investigated the case of fixed normal displacement of the indenter. It is also relevant to consider the opposite scenario, where the normal load F_n reached at the end of the loading phase is kept constant during tangential sliding. In reality, the boundary conditions are unlikely to remain strictly in either of these extreme cases, and an intermediate scenario is expected between fixed load and displacement conditions. In the following, we shall consider only short-range adhesion ($\mu_T = 6.08$), as it is of greater interest for rubber-like materials.

Figure 9a shows the normalized contact length $\hat{\mathcal{L}}$ as a function of the adimensional sliding speed $\hat{V}_s$. Results are given for different values of the maximum normal force reached at the end of the normal loading phase. This force is kept constant during the tangential sliding and steady-state results are reported. The trend of the contact length with the sliding speed is similar to the case of fixed displacement conditions (see Fig. 4a). Again, a maximum value of $\hat{\mathcal{L}}$ is obtained at intermediate speeds.

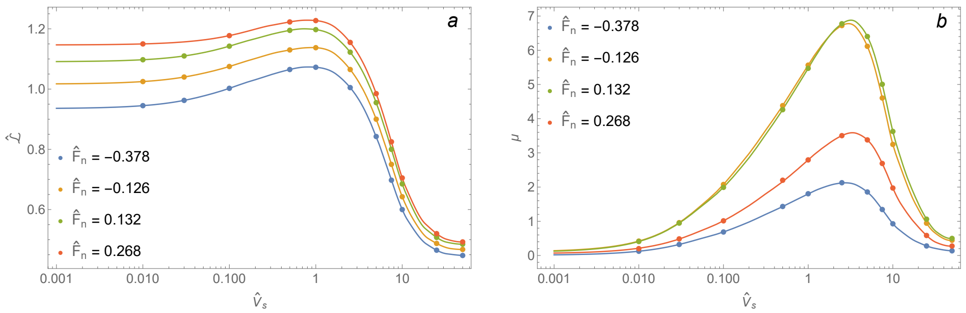

Fig. 9 The normalized contact length $\hat{\mathcal{L}}$ (a), and the viscoelastic friction coefficient μ (b) as a function of the adimensional sliding speed $\hat{V}_s$ for different values of the normal force $\hat{F}_n$. Plots are obtained under force-controlled conditions, and Tabor parameter $\mu_T = 6.08$. Solid circles represent numerical data returned by FEM simulations, while solid lines are obtained through a spline interpolation of these data.

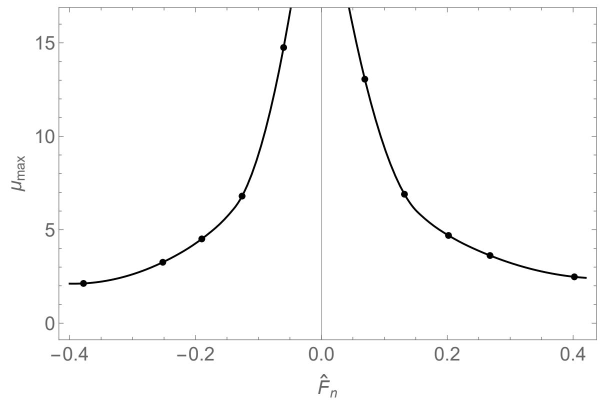

Fig. 10 Maximum friction coefficient μ_{max} as a function of the adimensional normal force $\hat{F}_n$ for a Tabor parameter $\mu_T = 6.08$ and under fixed normal-controlled conditions. Solid circles represent numerical data returned by FEM simulations, while solid lines are obtained through a spline interpolation of these data.

The viscoelastic friction coefficient exhibits a bell-shaped trend with respect to the sliding speed, as shown in Fig. 9b. Unlike the fixed displacement scenario (see Fig. 7b), in this case, the normal force does not change sign, and therefore, the friction coefficient cannot take unbounded values but reaches a maximum approximately within the speed range $\hat{V}_s = 2-4$, depending on the applied normal force. In this context, Fig. 10 shows the maximum friction coefficient μ_{max} as a function of $\hat{F}_n$, for a Tabor parameter $\mu_T = 6.08$. The friction coefficient exhibits a monotonically decreasing trend when the normal force is compressive (positive), whereas it increases with $\hat{F}_n$ when the normal force is negative (tensile), and is evidently unbounded at $\hat{F}_n = 0$. Moreover, we note that the minimum value of μ_{max} under negative forces is limited by the maximum tensile force occurring at pull-in, while, for compressive forces, it converges to the adhesiveless solution, as reported in Ref. [44].

These results align with the trends, reported in Ref. [57], concerning the variation of the friction coefficient with the normal force at fixed sliding speed. The data were obtained from experimental tests involving a rigid glass ball in adhesive contact on a smooth, flat rubber surface with an imposed relative motion.

3.3 Effect of the finite thickness of the substrate

The classical half-space approximation is widely utilized in contact mechanics, assuming that the contact area is significantly smaller than the size of the contacting bodies. However, real-world bodies possess finite thickness, which raises concerns regarding the applicability of the half-space model, particularly when dealing with highly compliant materials. In such cases, the mutual contact area can be comparable to or even larger than the thickness of the bodies involved. Despite their significant practical relevance, there are relatively few theoretical studies available for systems with finite thickness and many of them focus on sliding adhesiveless contact problems [60–62] or normal adhesive contacts [46–48].

Here, we extend our study to consider a rigid indenter sliding on a viscoelastic layer with a finite thickness t and in presence of adhesion. The degrees of freedom of the bottom nodes of the layer are rigidly coupled to simulate the confinement due to the presence of a rigid slab, a common assumption in scenarios such as the attachment of skin layers to bone [63]. Specifically, we investigate both cases of fixed normal displacement and normal load within the short-range adhesion regime.

Figure 11a illustrates the dimensionless contact length as a function of sliding speed for various thicknesses $\hat{t} = t/\epsilon$ of the viscoelastic layer, under controlled-displacement conditions. The increase in $\hat{\mathcal{L}}$ observed at intermediate speeds vanishes as the thickness decreases, with the contact region monotonically decreasing with $\hat{V}_s$. Additionally, rate-effects are less significant, as indicated by a flatter curve for thinner layers. This suggest a behaviour similar to that is observed in the long-range adhesive regime, where the contact becomes significantly stiffer with decreasing t [33, 47].

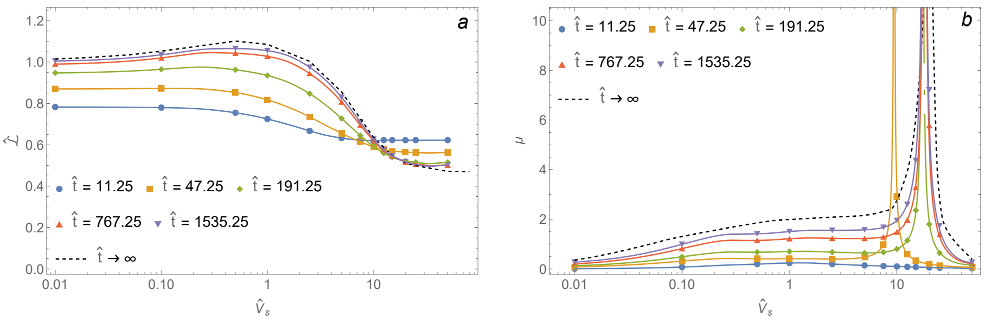

Fig. 11 The normalized contact length $\hat{\mathcal{L}}$ (a), and the viscoelastic friction coefficient μ (b) as a function of the adimensional sliding speed $\hat{V}_s$ for different values of the substrate thickness $\hat{t}$. Plots are obtained under displacement-controlled conditions for $\hat{\delta} = 3$, and Tabor parameter $\mu_T = 6.08$. Solid circles represent numerical data returned by FEM simulations, while solid lines are obtained through a spline interpolation of these data. The choice of the thickness values used is related to the mesh scheme employed to discretize the substrate.

Figure 11b illustrates the viscoelastic friction coefficient as a function of the sliding speed. Generally, μ decreases with thickness, consistent with theoretical predictions in the adhesionless case [17].

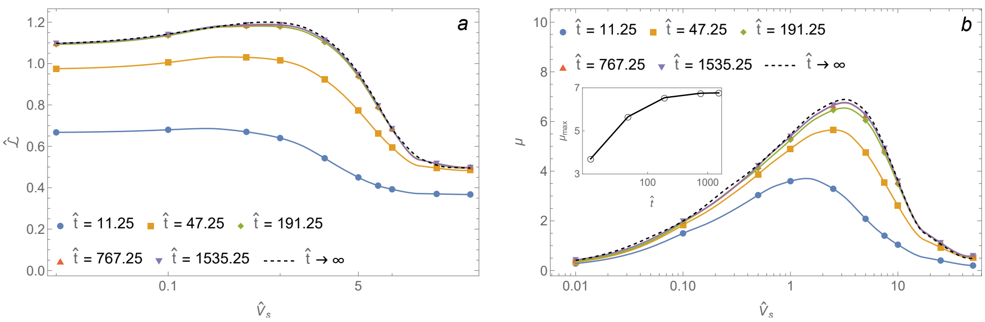

Fig. 12 The normalized contact length $\hat{\mathcal{L}}$ (a), and the viscoelastic friction coefficient μ (b) as a function of the adimensional sliding speed $\hat{V}_s$ for different values of the substrate thickness $\hat{t}$. Plots are obtained under normal force-controlled conditions for $\hat{F}_n = 0.134$, and Tabor parameter $\mu_T = 6.08$. Solid circles represent numerical data returned by FEM simulations, while solid lines are obtained through a spline interpolation of these data. The choice of the thickness values used is related to the mesh scheme employed to discretize the substrate. The inset in Fig. 12b illustrates the variation of the maximum friction coefficient with the thickness of the substrate in a Log-Linear plot.

When sliding occurs under fixed normal load conditions, the scenario changes as shown in Fig. 12, where the contact length $\hat{\mathcal{L}}$ and friction coefficient μ are plotted as functions of the sliding speed $\hat{V}_s$. We note that the qualitative behaviour of the contact length is not influenced by the normal boundary conditions (Fig. 12a), while the friction coefficient remains finite, as expected. Furthermore, the friction coefficient takes a maximum value, which increases with the thickness of the viscoelastic substrate, eventually reaching a plateau in the half-plane limit (see inset within Fig. 12b).

4 Conclusions

This study presents a comprehensive analysis of the sliding contact problem of a rigid Hertzian indenter on a viscoelastic substrate, emphasizing the effects of different adhesive regimes and boundary conditions (constant normal load and constant normal displacement). By employing a finite element method based on the formulation proposed by Afferrante & Violano [28], we accurately captured the viscoelastic behaviour of the substrate, and adhesion effects.

Our findings reveal that under long-range adhesion conditions, the normalized contact length decreases monotonically with increasing sliding speed (for both normal load and displacement control), converging to elastic solution values at low and high speeds. This indicates a transition in the substrate's stiffness due to its viscoelastic nature. Additionally, the viscoelastic friction coefficient exhibits a bell-shaped curve when the normal load is controlled, with the peak value influenced by the nature of the applied load. Under normal displacement control, the friction coefficient can become unbounded near a specific sliding speed, which corresponds to the normal force approaching zero. This critical behaviour is particularly important for understanding the limits and stability of displacement-controlled systems and suggests that friction can emerges also in absence of normal force.

In the short-range adhesion regime, the contact length initially increases with sliding speed, reaching a maximum before decreasing, indicating a transition from small-scale to large-scale viscous dissipation (as also shown in Ref. [30]).

Finally, we investigated the case of a viscoelastic layer with finite thickness bonded on a rigid foundation. In such case, rate-effects become less important when the thickness of the substrate is reduced. Due to the stiffening of the contact, a transition towards the long-range adhesive behaviour and a reduction of the friction coefficient with t are observed.

The significant influence of boundary conditions on the viscoelastic friction coefficient and contact length is evident, providing valuable insights for designing systems with tailored contact performance characteristics. The study also introduces a novel numerical methodology that simplifies the simulation of tangential displacement through vertical node movements, enhancing computational efficiency without sacrificing accuracy.

Acknowledgements

This work was partly supported by the Italian Ministry of University and Research under the Programme "Department of Excellence" Legge 232/2016 (Grant No. CUP - D93C23000100001) and by the European Union - NextGenerationEU through the Italian Ministry of University and Research under the programs: PRIN2022 (Projects of Relevant National Interest) grant nr. 2022SJ8HTC - ELectroactive gripper For mIcro-object maNipulation (ELFIN); PRIN2022 PNRR (Projects of Relevant National

Interest) grant nr. P2022MAZHX - TRibological modellIng for sustainaBle design Of induStrial friCtiOnal inteRfacEs (TRIBOSCORE).

References

[1] Lorenz, B., Persson, B., Fortunato, G., Giustiniano, M., Baldoni, F.: Rubber friction for tire tread compound on road surfaces. Journal of Physics: Condensed Matter **25**(9), 095007 (2013)

[2] Lorenz, B., Oh, Y., Nam, S., Jeon, S., Persson, B.: Rubber friction on road surfaces: Experiment and theory for low sliding speeds. The Journal of chemical physics **142**(19) (2015)

[3] Eddoumy, F., Addiego, F., Celis, J.-P., Buchheit, O., Berradja, A., Muller, R., Toniazzo, V., Ruch, D.: Reciprocating sliding of uniaxially-stretched ultra-high molecular weight polyethylene for medical device applications. Wear **272**(1), 50–61 (2011)

[4] Niemczyk, A., El Fray, M., Franklin, S.E.: Friction behaviour of hydrophilic lubricious coatings for medical device applications. Tribology International **89**, 54–61 (2015)

[5] Greiner, C., Schäfer, M.: Bio-inspired scale-like surface textures and their tribological properties. Bioinspiration & biomimetics **10**(4), 044001 (2015)

[6] Manoonpong, P., Petersen, D., Kovalev, A., Wörgötter, F., Gorb, S.N., Spinner, M., Heepe, L.: Enhanced locomotion efficiency of a bio-inspired walking robot using contact surfaces with frictional anisotropy. Scientific reports **6**(1), 39455 (2016)

[7] Peng, Y., Zeng, X., Liu, L., Cao, X., Zou, K., Chen, R.: Nanotribological characterization of graphene on soft elastic substrate. Carbon **124**, 541–546 (2017)

[8] Zeng, X., Peng, Y., Yu, M., Lang, H., Cao, X., Zou, K.: Dynamic sliding enhancement on the friction and adhesion of graphene, graphene oxide, and fluorinated graphene. ACS applied materials & interfaces **10**(9), 8214–8224 (2018)

[9] Meyer, D.J., Peshkin, M.A., Colgate, J.E.: Fingertip friction modulation due to electrostatic attraction. In: 2013 World Haptics Conference (WHC), pp. 43–48 (2013). IEEE

[10] Ayyildiz, M., Scaraggi, M., Sirin, O., Basdogan, C., Persson, B.N.: Contact mechanics between the human finger and a touchscreen under electroadhesion. Proceedings of the National Academy of Sciences **115**(50), 12668–12673 (2018)

[11] Santeramo, M., Putignano, C., Vorlaufer, G., Krenn, S., Carbone, G.: On the

role of viscoelasticity in polymer rolling element bearings: Load distribution and hysteretic losses. Mechanism and Machine Theory **189**, 105421 (2023)

[12] Christensen, R.M.: Theory of Viscoelasticity. Courier Corporation, ??? (2003)

[13] Johnson, K.L.: Contact Mechanics. Cambridge university press, ??? (1987)

[14] Popov, V.L., *et al.*: Contact Mechanics and Friction. Springer, ??? (2010)

[15] Barber, J.R.: Contact Mechanics. Springer, ??? (2018)

[16] Hunter, S.: The rolling contact of a rigid cylinder with a viscoelastic half space (1961)

[17] Margetson, J.: Rolling contact of a rigid cylinder over a smooth elastic or viscoelastic layer. Acta Mechanica **13**(1), 1–9 (1972)

[18] Persson, B.: Rolling friction for hard cylinder and sphere on viscoelastic solid. The European Physical Journal E **33**, 327–333 (2010)

[19] Menga, N., Putignano, C., Carbone, G., Demelio, G.: The sliding contact of a rigid wavy surface with a viscoelastic half-space. Proceedings of the Royal Society A: Mathematical, Physical and Engineering Sciences **470**(2169), 20140392 (2014)

[20] Menga, N., Afferrante, L., Demelio, G., Carbone, G.: Rough contact of sliding viscoelastic layers: numerical calculations and theoretical predictions. Tribology International **122**, 67–75 (2018)

[21] Persson, B.N.: Theory of rubber friction and contact mechanics. The Journal of Chemical Physics **115**(8), 3840–3861 (2001)

[22] Sukhomlinov, S., Müser, M.H.: On the viscous dissipation caused by randomly rough indenters in smooth sliding motion. Applied Surface Science Advances **6**, 100182 (2021)

[23] Gent, A.: Adhesion and strength of viscoelastic solids. is there a relationship between adhesion and bulk properties? Langmuir **12**(19), 4492–4496 (1996)

[24] Lorenz, B., Krick, B., Mulakaluri, N., Smolyakova, M., Dieluweit, S., Sawyer, W., Persson, B.: Adhesion: role of bulk viscoelasticity and surface roughness. Journal of Physics: Condensed Matter **25**(22), 225004 (2013)

[25] Tiwari, A., Dorogin, L., Bennett, A., Schulze, K., Sawyer, W., Tahir, M., Heinrich, G., Persson, B.: The effect of surface roughness and viscoelasticity on rubber adhesion. Soft matter **13**(19), 3602–3621 (2017)

[26] Violano, G., Chateauminois, A., Afferrante, L.: Rate-dependent adhesion of viscoelastic contacts, part i: Contact area and contact line velocity within model

randomly rough surfaces. Mechanics of Materials **160**, 103926 (2021)

[27] Van Dokkum, J.S., Pérez-Rafols, F., Dorogin, L., Nicola, L.: On the retraction of an adhesive cylindrical indenter from a viscoelastic substrate. Tribology International **164**, 107234 (2021)

[28] Afferrante, L., Violano, G.: On the effective surface energy in viscoelastic hertzian contacts. Journal of the Mechanics and Physics of Solids **158**, 104669 (2022)

[29] Müser, M.H., Persson, B.N.: Crack and pull-off dynamics of adhesive, viscoelastic solids. Europhysics Letters **137**(3), 36004 (2022)

[30] Carbone, G., Mandriota, C., Menga, N.: Theory of viscoelastic adhesion and friction. Extreme Mechanics Letters **56**, 101877 (2022)

[31] Papangelo, A., Ciavarella, M.: Detachment of a rigid flat punch from a viscoelastic material. Tribology letters **71**(2), 48 (2023)

[32] Violano, G., Chateauminois, A., Afferrante, L.: Rate-dependent adhesion of viscoelastic contacts. part ii: Numerical model and hysteresis dissipation. Mechanics of Materials **158**, 103884 (2021)

[33] Violano, G., Afferrante, L.: On the long and short-range adhesive interactions in viscoelastic contacts. Tribology Letters **70**(3), 68 (2022)

[34] Persson, B.N., Scaraggi, M.: Theory of adhesion: Role of surface roughness. The Journal of chemical physics **141**(12) (2014)

[35] Thimons, L.A., Gujrati, A., Sanner, A., Pastewka, L., Jacobs, T.D.: Hard-material adhesion: Which scales of roughness matter? Experimental Mechanics **61**(7), 1109–1120 (2021)

[36] Violano, G., Demelio, G.P., Afferrante, L.: On the dmt adhesion theory: from the first studies to the modern applications in rough contacts. Procedia Structural Integrity **12**, 58–70 (2018)

[37] Johnson, K.L., Kendall, K., Roberts, A.: Surface energy and the contact of elastic solids. Proceedings of the royal society of London. A. mathematical and physical sciences **324**(1558), 301–313 (1971)

[38] Israelachvili, J.N., McGuiggan, P.M.: Adhesion and short-range forces between surfaces. part i: New apparatus for surface force measurements. Journal of Materials Research **5**(10), 2223–2231 (1990)

[39] Tabor, D.: Surface forces and surface interactions. In: Plenary and Invited Lectures, pp. 3–14. Elsevier, ??? (1977)

[40] Afferrante, L., Violano, G., Dini, D.: How does roughness kill adhesion? Journal

of the Mechanics and Physics of Solids **181**, 105465 (2023)

[41] Afferrante, L., Violano, G., Carbone, G.: Exploring the dynamics of viscoelastic adhesion in rough line contacts. Scientific Reports **13**(1), 15060 (2023)

[42] Pérez-Ràfols, F., Nicola, L.: Incipient sliding of adhesive contacts. Friction, 1–14 (2022)

[43] Mandriota, C., Menga, N., Carbone, G.: Adhesive contact mechanics of viscoelastic materials. International Journal of Solids and Structures **290**, 112685 (2024)

[44] Papangelo, A., Nazari, R., Ciavarella, M.: Friction for a sliding adhesive viscoelastic cylinder: Effect of maugis parameter. European Journal of Mechanics-A/Solids, 105348 (2024)

[45] Menga, N., Afferrante, L., Carbone, G.: Adhesive and adhesiveless contact mechanics of elastic layers on slightly wavy rigid substrates. International Journal of Solids and Structures **88**, 101–109 (2016)

[46] Violano, G., Afferrante, L.: Size effects in adhesive contacts of viscoelastic media. European Journal of Mechanics-A/Solids **96**, 104665 (2022)

[47] Violano, G., Afferrante, L.: Unraveling adhesion mechanisms: Exploring the impact of thickness on viscoelastic layers and wavy profiles. Tribology Letters **72**(1), 14 (2024)

[48] Maghami, A., Tricarico, M., Ciavarella, M., Papangelo, A.: Viscoelastic amplification of the pull-off stress in the detachment of a rigid flat punch from an adhesive soft viscoelastic layer. Engineering Fracture Mechanics **298**, 109898 (2024)

[49] Putignano, C., Menga, N., Afferrante, L., Carbone, G.: Viscoelasticity induces anisotropy in contacts of rough solids. Journal of the Mechanics and Physics of Solids **129**, 147–159 (2019)

[50] Raous, M.: Interface models coupling adhesion and friction. Comptes Rendus Mecanique **339**, 491–201 (2011)

[51] Derjaguin, B.: Untersuchungen ueber die reibung und adhaesion, iv: Theorie des anhaftens kleiner teilchen. Kolloid-Zeitschrift **69**, 155–164 (1934)

[52] Greenwood, J.: Adhesion of elastic spheres. Proceedings of the Royal Society of London. Series A: Mathematical, Physical and Engineering Sciences **453**(1961), 1277–1297 (1997)

[53] Feng, J.Q.: Contact behavior of spherical elastic particles: a computational study of particle adhesion and deformations. Colloids and Surfaces A: Physicochemical and Engineering Aspects **172**(1-3), 175–198 (2000)

[54] Feng, J.Q.: Adhesive contact of elastically deformable spheres: a computational study of pull-off force and contact radius. Journal of colloid and interface science **238**(2), 318–323 (2001)

[55] Carbone, G., Putignano, C.: A novel methodology to predict sliding and rolling friction of viscoelastic materials: Theory and experiments. Journal of the Mechanics and Physics of Solids **61**(8), 1822–1834 (2013)

[56] Afferrante, L., Putignano, C., Menga, N., Carbone, G.: Friction in rough contacts of linear viscoelastic surfaces with anisotropic statistical properties. The European Physical Journal E **42**, 1–8 (2019)

[57] Barquins, M.: Adherence, friction and wear of rubber-like materials. Wear **158**, 87–117 (1992)

[58] Barquins, M., Maugis, D., Blouet, J., Courtel, R.: Contact area of a ball rolling on an adhesive viscoelastic material. Wear **51**(2), 375–384 (1978)

[59] Charmet, J.-C., Barquins, M.: Adhesive contact and rolling of a rigid cylinder under the pull of gravity on the underside of a smooth-surfaced sheet of rubber. International journal of adhesion and adhesives **16**(4), 249–254 (1996)

[60] Putignano, C., Carbone, G., Dini, D.: Mechanics of rough contacts in elastic and viscoelastic thin layers. International Journal of Solids and Structures **69**, 507–517 (2015)

[61] Menga, N., Afferrante, L., Carbone, G.: Effect of thickness and boundary conditions on the behavior of viscoelastic layers in sliding contact with wavy profiles. Journal of the Mechanics and Physics of Solids **95**, 517–529 (2016)

[62] Menga, N., Afferrante, L., Demelio, G., Carbone, G.: Rough contact of sliding viscoelastic layers: numerical calculations and theoretical predictions. Tribology International **122**, 67–75 (2018)

[63] Jobanputra, R., Boyle, C., Dini, D., Masen, M.: Modelling the effects of age-related morphological and mechanical skin changes on the stimulation of tactile mechanoreceptors. Journal of the Mechanical Behavior of Biomedical Materials **112**, 104073 (2020)